Journal of African Earth Sciences 206 (2023) 105020

Contents lists available at ScienceDirect

Journal of African Earth Sciences

journal homepage: www.elsevier.com/locate/jafrearsci

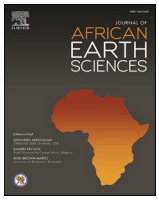

Geospatial modelling of mineral potential zones using data-driven based weighting factor and statistical index techniques

Prince Ofori Amponsah [a], Eric Dominic Forson [b,*]

[a] Department of Earth Science, School of Physical and Mathematical Sciences, University of Ghana, P.O. Box LG 58, Legon, Accra, Ghana
[b] Department of Physics, School of Physical and Mathematical Sciences, University of Ghana, P. O. Box LG 63, Legon, Accra, Ghana

ARTICLE INFO

Keywords:
Mineral prospectivity modelling
Weighting factor
Statistical index
Area under receiver operating characteristics
Geophysical datasets

ABSTRACT

Mineral prospectivity models (MPMs) are significantly essential in delineating target zones with the optimum likelihood of containing a particular sought-after mineral deposit. This present study carried out mineral potential mapping over the Collette Prospecting Licence (PL) Area of north-western Ghana using bivariate data-driven spatial statistical models composed of statistical index (SI) and weighting factor (WF) approaches. In the first instance, the geographic coordinates of variously known locations of artisanal mining operations as well as high Au concentration locations were mapped during a field survey. As a result, 181 known locations of Au occurrences were identified, out of which 127 (70%) were selected randomly for training and creating the mineral prospectivity models, whereas the remaining 54 (30%) were used to assess and validate the accuracy of the predictive models produced. The efficacy of mineral prospectivity models generated enormously depends on the appropriate selection of mineral-related factors. In this study, the following mineral-related condition factors (evidential layers) comprising analytic signal, lineament density, uranium-thorium ratio, uranium, potassium-thorium ratio, potassium, reduction-to-equator, and geology were used. The aforementioned evidential layers were derived and sourced from geophysical and geological datasets, which were later prepared for the generation of the models in a geographic information systems (GIS) environment. Finally, the validation of the mineral prospectivity models generated was carried out by applying the receiver operating characteristics (ROC) curve. The estimated results based on the ROC plots obtained for the predictive models showed that the area under the ROC curve (AUC) scores obtained for the SI-based and WF-based mineral prospectivity models were respectively, 0.780 and 0.733. Hence, it can be concluded that both mineral predictive models created in this study produced reasonably good accuracy (AUC score greater than 0.7) in predicting the potential zones of gold mineralisation occurrences within the Collette PL Area of north-western Ghana. These MPMs can serve as essential models for mineral exploration programmes within the study area.

1. Introduction

Mineral prospecting fundamentally concerns the exploration and delineation of new areas characterised by ore-bearing minerals over a specified region of interest. The aforementioned basis for mineral prospecting dwells on differentiating highly prospective zones from prospectively low regions of a particular sought-after mineral within the area explored. In carrying out predictive modelling over a specified area based on the objective of delineating new zones that are prospectively characteristic of the target mineral, various geospatial exploratory datasets comprising geophysical, geological, and geochemical layers ought to be acquired, analysed, and synthesised. This makes the generation of mineral prospectivity models (MPM) a multi-criteria decision-making (MCDM) activity whose output outlines prospective zones of mineral occurrence (e.g., Carranza and Laborte, 2015; Yousefi and Carranza, 2015; Kashani et al., 2016; Forson et al., 2020; Forson and Menyeh, 2023). In synthesising geospatial datasets towards the generation of a predictive model in a geoscientific context, many approaches have been developed and have been generally grouped into knowledge-driven and data-driven approaches (e.g., McKay and Harris, 2016; Sun et al., 2020; Parsa and Carranza, 2021; Zhang et al., 2021; Amponsah et al., 2022a,b; Forson et al., 2022b). Predictive modelling that employs the knowledge-driven technique solicits the opinions of geoscience experts in relation to the sought-after natural resource

* Corresponding author.
E-mail addresses: edforson@ug.edu.gh, ericdforson@gmail.com (E.D. Forson).

https://doi.org/10.1016/j.jafrearsci.2023.105020
Received 16 January 2023; Received in revised form 14 July 2023; Accepted 28 July 2023
Available online 1 August 2023

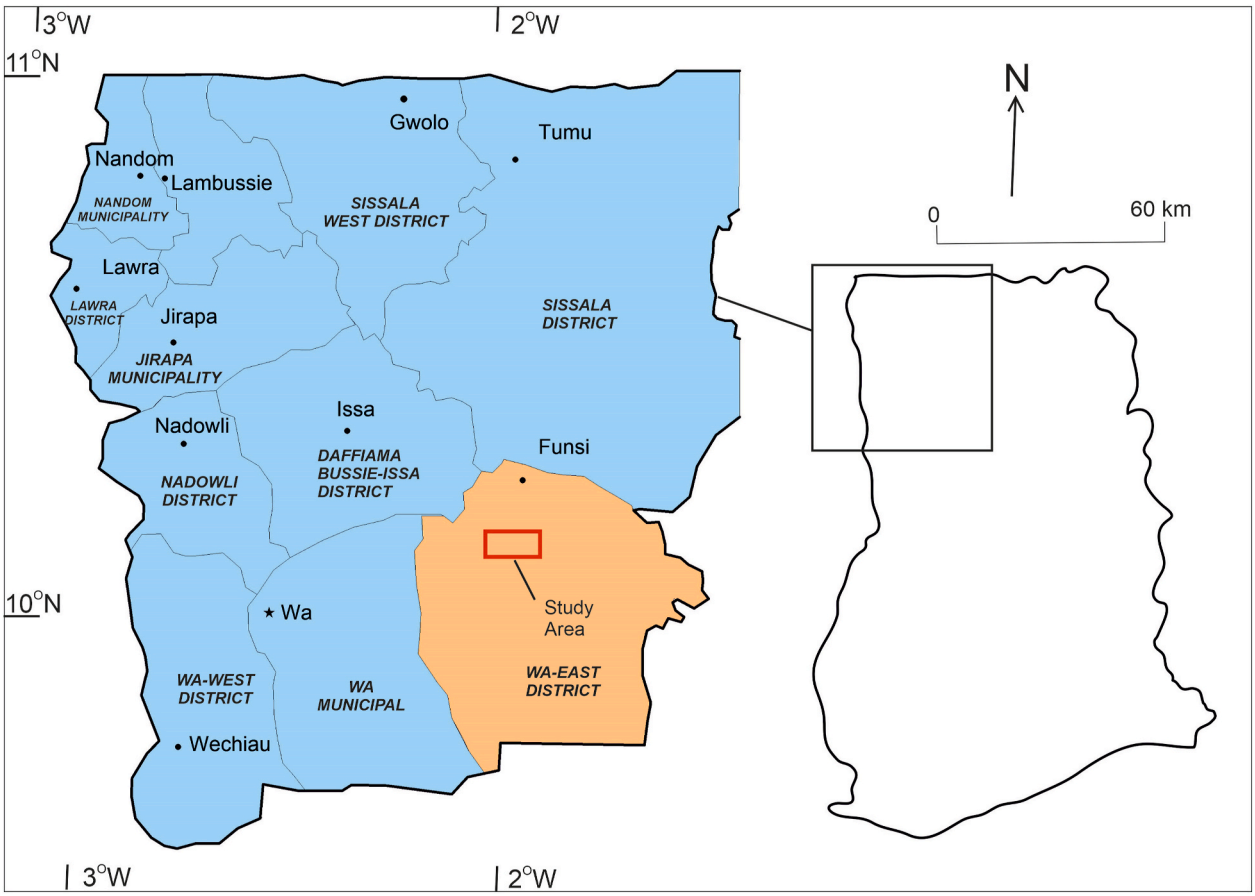

Fig. 1. Map of the north-western Ghana showing various administrative districts (Study area is marked in red).

(mineral, groundwater, etc.) to assign weights to various geoscientific-derived evidential layers that are to be integrated to generate the model. Commonly used knowledge-driven approaches in geospatial predictive modelling that have been applied in recent literature comprise of the analytical hierarchy process (Barati et al., 2018; Akinlalu et al., 2021), the fuzzy analytical hierarchy process (Forson et al., 2020; Khosravi et al., 2021), fuzzy logic (Sanusi and Amigun, 2020; Abdelkareem and Al-Arifi, 2021), and the technique for order preference by similarity to the ideal solution (TOPSIS) (Mansouri et al., 2017; Rahimi et al., 2020). The other category of data synthesis techniques (known as the data-driven method) employed in predictive modelling determines the spatial correlation between each of the evidential layers used with respect to the known location of the occurrence of the sought-after natural resource (such as gold, copper, and water). Thus, in the data-driven method, known locations of occurrence of the sought-after mineral are employed as training points to determine the weight or influence of each of the evidential layers to be incorporated in the predictive model to be produced (Carranza, 2008; Forson et al., 2022b). In view of this, a fundamental drawback in the application of data-driven approaches is the unavailability of known locations of the sought-after minerals locally at the deposit scale. However, when employed over regions where a considerable amount of known mineral occurrences are found, these data-driven methods are able to generate objective weights for the evidential layers to be integrated rather than relying on expert opinions as in the case of knowledge-driven approaches. Examples of data-driven MPM techniques include frequency ratio (Mathew and Ariffin, 2018; Kusuma et al., 2019), weight of evidence (Zhang et al., 2016; Fu et al., 2021), evidence belief function (Carranza, 2015; Ford et al., 2016), statistical index (Ghasemzadeh et al., 2022), weighting factor (Esmaeiloghli et al., 2021), Shannon entropy (Al-Abadi, 2017), and machine learning methods (Lin et al., 2021; Zhenjie et al., 2021; Zhang et al., 2022).

The study focuses on identifying locations for areas for exploratory drilling within a large region in the Collette PL Area of the Northwestern part of Ghana by incorporating diverse evidential layers sourced from geological and geophysical datasets. Furthermore, this study compares the performance of mineral prospectivity models that would be generated based on the use of data-driven statistical techniques comprising weighting factor (WF) and statistical index (SI) approaches that have been successfully employed in determining the influence of various evidential layers that are to be integrated into a prospectivity model in various geoscience contexts (Meinhardt et al., 2015; Khosravi et al., 2016).

2. Study area and geological setting

2.1. Study area

The Collette Prospecting Licence Area is located approximately 800 km NNW of Accra in the Upper West region of Ghana, specifically the Wa-East district (Fig. 1). The area lies within longitudes 2°06′ and 2°01′ and latitudes 10°9′ and 10°5’ using the WGS datum ellipsoid. The regional capital of Wa is located 60 km southeast of the tenement. There are no communities in the tenement area. Access from Wa is through the Wa-Sandema road to Bulenga, and south of the prospecting licence area, access is via networks of graded laterite roads that link the major towns and small villages. There are also several poorly graded third-class laterite roads that become impassable during the peak periods of the June to October wet season. The area is relatively flat, with low east-west rolling hills occupying the Julie belt. The climate in the arid Sahel Belt of northern Ghana is characterised by annual rainfall between 1000–1250 mm/year, largely falling in the rainy season from June to

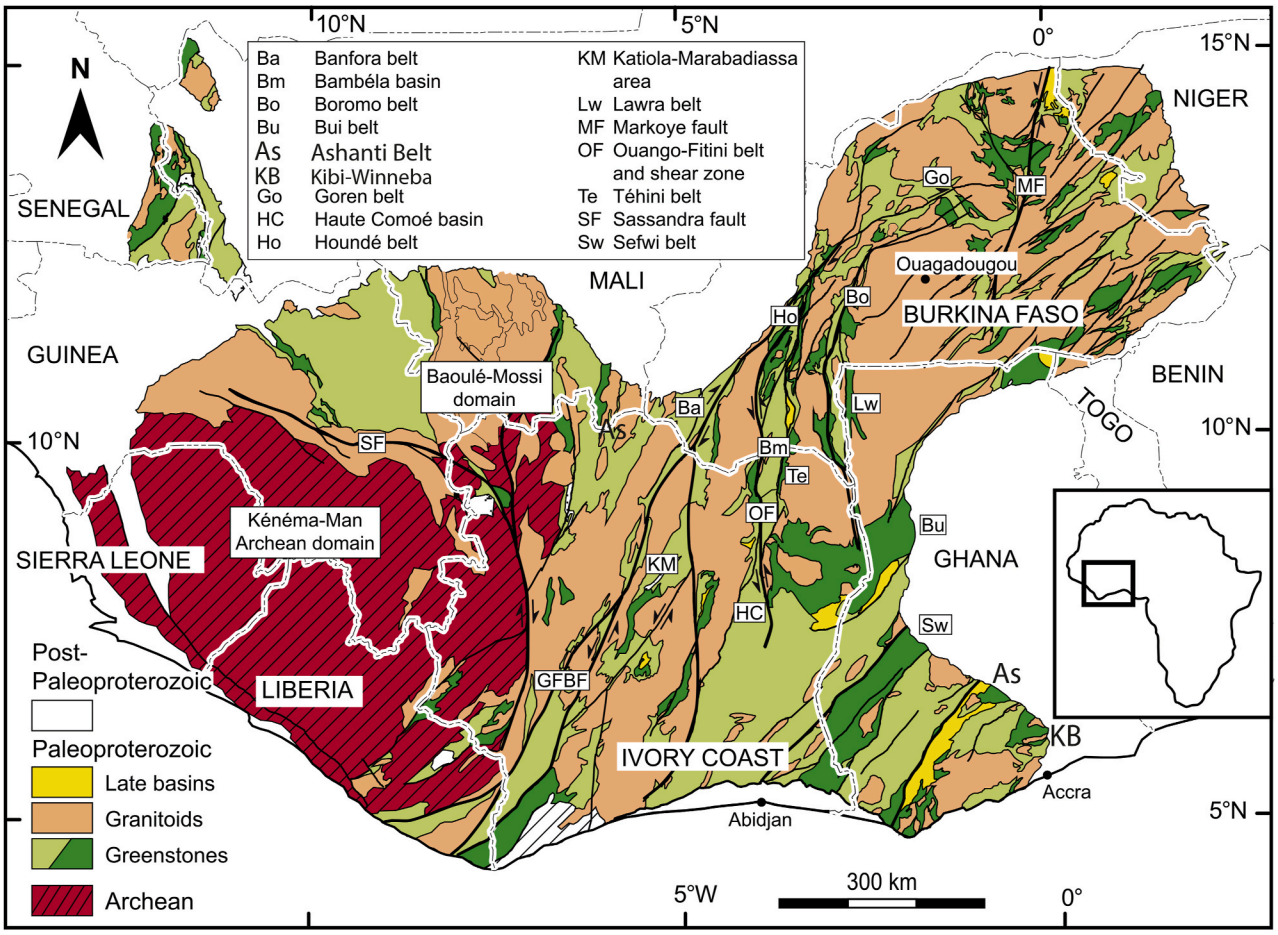

Fig. 2. Map of the west african craton (WAC).

October (that peaks in August–September; Dickson and Benneh (1988)).

2.2. Regional geology of the study area

The Precambrian West African shield is composed of both Archean and Paleoproterozoic nuclei, which form two major domains known as the Reguibet shield (nWAC) to the north and the Leo-Man shield (sWAC) to the south. The Archean portion of the sWAC is termed the Kénéma Man Shield, and the Paleoproterozoic portion is termed the Birimian or the Baoulé-Mossi domain (Rocci, 1965; Baratoux et al., 2011; Block et al., 2016; Masurel et al., 2022). The Birimian domain crops out in countries such as Ghana, Burkina Faso, Mali, Niger, Mali, Senegal, Ivory Coast, and Guinea (Jessell et al., 2012; Amponsah et al., 2015; Diatta et al., 2017; Eglinger et al., 2017; Feng et al., 2018), and it is composed of arcuate granite-greenstone belts and sedimentary basins (Feng et al., 2019). In Ghana, there are six (6) of these arcuate granite-greenstone belts, namely the Kibi-Winneba belt, the Ashanti belt, the Sefwi belt, the Bui belt, the Bole-Navrongo belt, and the Wa-Lawra belt, and architecturally, all the belts have a northeast-southwest structural grain (Fig. 2; Agra et al., 2023), except for the Wa-Lawra Belt, which has a north-south orientation and is part of the larger Boromo belt, which extends into Burkina Faso (Amponsah et al., 2016; Salvi et al., 2016; Feng et al., 2019; Sapah et al., 2021; Nunoo et al., 2022; Amponsah et al., 2023). The geology of northwest Ghana is defined by the north-south oriented Wa-Lawra belt and the northeast-southwest oriented Bole-Nangodi greenstone belts that meet at a tangent in northwestern Ghana. The Wa-Lawra greenstone belt is composed of metasedimentary rocks (mainly shales and greywackes), metavolcanics (basically basalts, rhyolites, and andesites), and intrusive granitoids. According to Agyei-Duodu (2009) the metasediments were deposited around 2139 ± 2 Ma, with the late intrusive granitoids around 2104 ± 1 Ma. Juxtaposing the Wa-Lawra to the east is the Koudougou-Tumu domain, bounded by the Jirapa shear zone. This domain is composed of high-grade granulite facies 2187 ± 3 Ma to 2165 ± 7 Ma granitoid genies, biotite schist, 2134 ± 1 Ma hornblende-biotite tonalite, and 2124 ± 2 Ma biotite hornblende monzodiorite. These rocks have been intruded by late plutonic suites composed of 2112 ± 1 Ma biotite granite, 2106 ± 1 Ma biotite granite, hornblende biotite tonalite, and quartz diorite (Agyei-Duodu, 2009; Block et al., 2016; Amponsah et al., 2016). Lying east-west within the Koudougou-Tumu domain is the Julie Belt. This belt is composed of basalt, andesite, and volcaniclastic sediments. They are marked by allochthonous bodies or thrust nappes as a result of low-angle thrust faults, with the fault planes developing shear zones that host the Julie gold mineralisation (Amponsah et al., 2015; Block et al., 2016; Nunoo et al., 2022) as well as the Collette main deposit (Azumah Resources Limited, 2018). South of the Julie belt is the Bole-Bulenga domain. This domain is composed of 2150 ± 4 Ma biotite granitoid, k-feldspar-rich granitoid, and hornblende tonalite. These rocks are overlain by patches of Tarkwaian detrital sediments composed of sandstones and conglomerates. These detrital sediments are highly rich in magnetite. South and southeast of the Bole-Bulenga domain and the Koudougou-Tumu domain (Fig. 3a), respectively, is the crustal-scale Bole-Nangodi greenstone belt. The main structural grain of this shear zone is northeast-southwest. The belt is composed of 2179 ± 2 Ma to 2156 ± 1 Ma hornblende biotite granitoid, 2159 ± 4 Ma volcaniclastic sediments, 2139 ± 2 Ma wacke-dominated sediment, basalts, andesites, rhyolites, and banded manganese formations. These rocks have been intruded by late 2112 ± 2 Ma hornblende biotite tonalites, 2120 ± 1 Ma

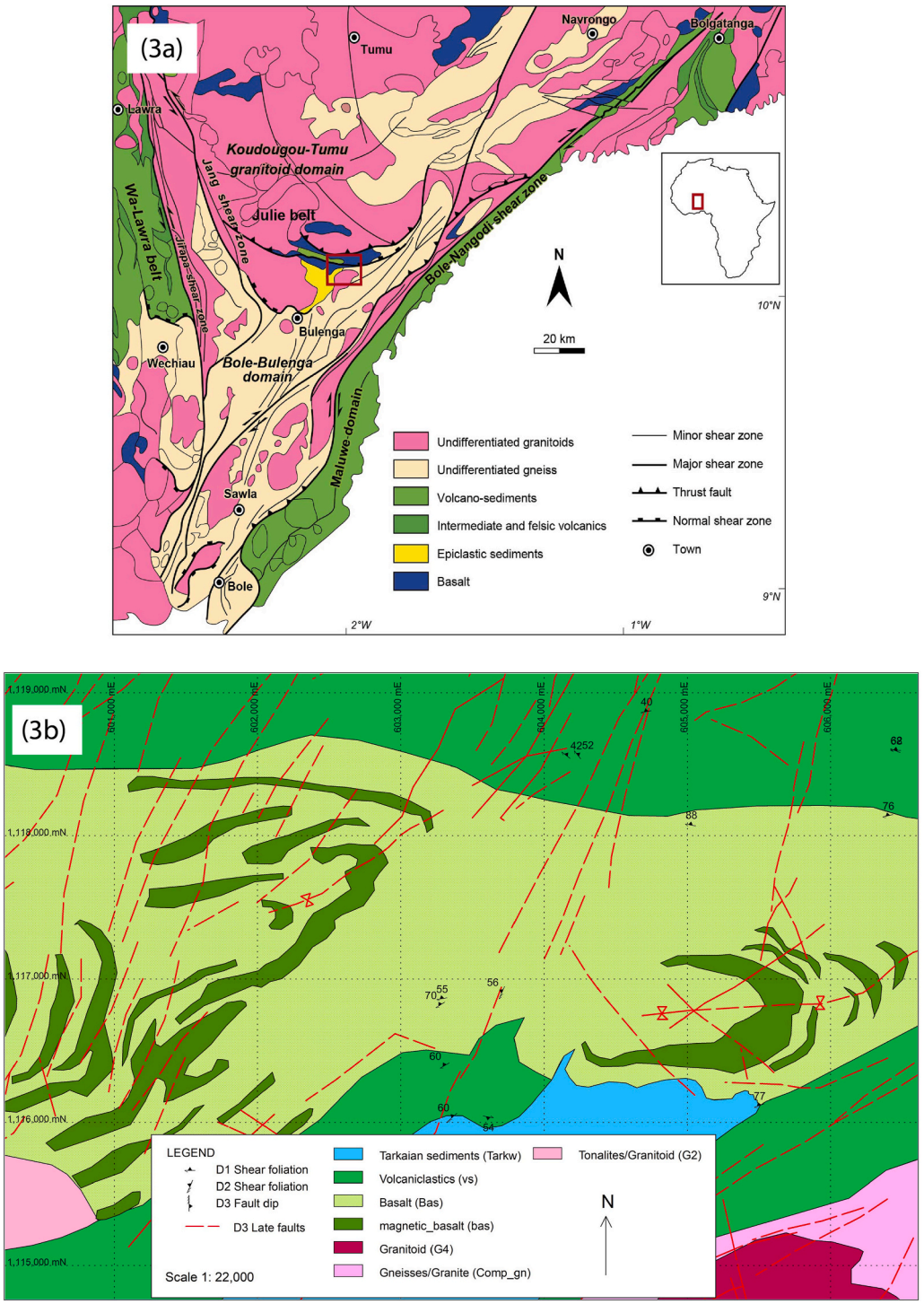

Fig. 3. (a) Regional geological map of the north-western Ghana showing the study area in red (modified after Amponsah et al., 2015) (b) simplified geological map of the study area (thus the Collette tenement) showing the lithologies and structural measurement.

biotite muscovite granites, and 2134 ± 6 Ma tonalites (Agyei-Duodu, 2009). The southern margins of this belt have been covered by the Neoproterozoic Volta Basin sediments (Fig. 3a).

2.3. Structural framework of the study area

The summary of the structural disposition of the Collette deposit is mainly from the work of Amponsah et al. (2015) and Block et al. (2016). Architecturally, the Collette deposit, just like the Julie deposit, is located on the E-W shear zone of the Julie belt, but the former occurs at a structural junction where the E-W oriented dextral jog shear zone of the Julie belt tangentially meets the NE trending shear zone of the Bole-Bulenga domain. The E-W oriented shear zone, which is denoted by the N–S shortening in the Julie belt, marks the initial deformation (D1) in the Julie belt, which was formed as a result of the nappe stacking event that affected all the rocks in the belt (Amponsah et al., 2015). This shear zone dips 35–70° to the north, and the L1 lineation trends 025° with plunges between 35° to 80°. Boudinage syn-deformational quartz veins oriented in the direction of (or parallel to) the E-W shear zone were observed. In the volcaniclastic rocks, F1 vertical plunging folds verging

towards the east form E-W trending shear foliation, which is parallel to the axial plane of the F1 folds.

The NE trending shear zone Bole-Bulenga domain, according to Block et al. (2016), marks a N–S directed extension event and represents a second deformational event (D2) that affected all the rocks in the study area. This shear zone denotes the boundary between the low-grade Julie belt and the high-grade Bole-Bulenga domain. This shear zone has dips ranging from 40 to 50° to the north and has affected the Tarkwaian polymitic conglomerates and the high-strained migmatitic, ortho-, and *para*-gniesses. L2, which is stretching mineral lineation found on the shear zones or foliation, trends north with a 20° plunge. Both shear zones exhibit brittle-ductile transition characteristics with deformed north-side-up sigmoidal shear zone indicators (mainly from rotated, deformed mineral fabrics with pressure shadows).

The third deformation (D3) event observed in the study area is a brittle late-stage event marked by NE-SW and NW-SW shortening events represented by the numerous late NE-SW and NW-SE oriented faults with dips ranging from 36° to 60° to the NW (Fig. 3b; Amponsah et al., 2015).

2.4. Mineralisation style of the study area

The mineralisation in Collette is predominantly quartz vein-hosted, which occurs within metavolcaniclastics rocks (vs) and sheared potassic-altered granites and gneisses (comp-gn). Primarily, the meta-volcaniclastic rocks are composed of shale and siltstone facies with its mineralogy composed of quartz and minor k-felspars, and that of the comp-gn is composed of plagioclase, hornblende, and biotite with accessory minerals composed of titanite, perthitic alkali feldspars, and zircon (Amponsah et al., 2015; Azumah Resources Limited, 2018). The comp-gn has a primary tonalitic composition overprinted by a migmatitic metamorphic assemblage of epidote, calcite, fine-grained biotite, and rutile, and that of the volcaniclastics are graphite, calcite, and chlorite. This mineral assemblage is characteristic of greenschist facies and indicates that the mineralisation is under greenschist facies conditions. Meso- and micro-structural analysis during geological mapping and drill core logging in the Collette Prospective Licence Area identified three main deformational events, which coincide with the D1, D2, and D3 phases described by Block et al. (2016) and Amponsah et al. (2015). Gold mineralisation at Collette occurs as micron-sized inclusions and free gold within fractures of euhedral pyrites that have precipitated within fracture-controlled crystalline quartz-carbonate-tourmaline veins associated with D1 within the sheared comp-gn as well as transposed quartz veins that occur within the east -west shear zone that has affected the volcaniclastic rocks (vs) and the Tarkwaian sediments (Tarkw). Gold in the comp-gn rocks is associated with other metals and REE minerals within pyrite grains such as silver, bismuth, tellurium, xenotime, bastnäsite, and trace amounts of base metals such as copper and lead (Amponsah et al., 2015). The ore body defined in Collette is made up of a series of plunging ore shots (mostly likely of cylindrical shape) which trend E-W and dip between 50° and 70° to the north. The bulk of the gold inventory is found at the intersection between the E-W shear zone defined by the Julie structural grain and the northeast structure defined by the Bole-Bulenga domain. The ore thickness ranges from 10 to 20 m. The sulphide assemblage in the gold-bearing quartz veins is dominated by pyrite in the tonalites and arsenopyrites in the sediments. In the comp-gn, the pyrite occurs as single euhedral crystals, disseminated grains within vein alteration selvedges, and irregularly shaped “clots”. Chalcopyrite is quite rare and is interpreted to have formed at the same time as pyrite (and gold; Amponsah et al. (2015)). The bulk of the gold inventory, as well as high-grade mineralisation, is found at the intersection between the D1 E-W shear zone and the D3 late northeast or northwest brittle faults. The ore thickness ranges from 10 to 20 m.

3. Methodology

3.1. Geoscientific database construction using GIS

The fundamental procedure of a mineral prospectivity model is the collection of spatial data and the creation of a geospatial database from which the essential mineral-based geoscientific evidential layers can be derived. A geospatial database comprising associated factors of the sought-after mineral was created in this study. It is noteworthy that the reliability of a mineral prospectivity model (MPM) produced is enormously dependent on the quality and quantity of data available, the chosen scale for the study area, the appropriate factors chosen as well as the data integration methods selected for the analysis and modelling. In view of this, eight geoscientific evidential layers comprising the analytic signal, lineament density, lithology, potassium (K) concentration, potassium-thorium (K-eTh) ratio, magnetic intensity-based reduction-to-equator (RTE), uranium (eU) concentration, and uranium-thorium (eU-eTh) ratio were generated from airborne magnetic, airborne radiometric, and geological datasets. The magnetic and radiometric datasets were obtained from Azumah Resources Limited (ARL; Azumah Resources Limited, 2018). The radiometric-based evidential layers, which number up to four layers (K concentration, K-eTh ratio, eU concentration and eU-eTh ratio), were generated by using the minimum curvature gridding method to grid K and eU concentration channels in Geosoft Oasis Montaj software. This aforementioned software was also used to generate the two ratio layers (K-eTh and eU-eTh ratios). In the case of the airborne magnetic data, the magnetic intensity data acquired over the study area was first gridded using the minimum curvature gridding method. Since the study area is in a low magnetic latitude zone, the observed magnetic intensity values and their corresponding geological responses are asymmetric in nature. Thus, the reduction-to-equator filter was applied to the magnetic intensity grid so as to remove the asymmetric effects associated with magnetic intensity datasets collected at low magnetic latitudes. Subsequently, the reduction-to-equator evidential layer was generated, which characterises a symmetric distribution of magnetic responses over their respective sources. The analytic signal layer was created by applying the analytic signal filter to the magnetic intensity grid. The CET (Centre for Exploration Targeting) grid analysis technique was applied to the RTE layer to generate the lineament density layer that outlines the intensity of occurrence of lineaments such as dikes, faults, fractures, etc. over a region of interest. All the evidential layers sourced from the geophysical datasets (magnetic and radiometric) were pre-processed and processed in the Geosoft Oasis Montaj software. These aforesaid geophysically-extracted layers were then exported to raster format for further processing in ArcGIS 10.8. The geological layer (Fig. 3b), which comprises various lithological classes within the study area, was extracted from geological data compiled by the Ghana Geological Survey Authority (Agyei-Duodu, 2009) in vector shapefile format. In order to ensure that all evidential layers are in the appropriate format for further processing and analysis, the geology layer was also converted to a raster format. The lithological classes within the study area comprise bas (basalts), comp-gn (granite/gneisses), G2 (tonalite/granitoid), G4 (granitoid), tarkw (Tarkwaian sediments), and vs (volcaniclastic sediments with siltstone and shale facies). Afterwards, the evidential layers were imported into a GIS environment (ArcGIS 10.4 and ArcGIS Pro) for further processing and rescaling towards the attainment of the same cell size of 2 m (yielding a total area pixel count of 10,630,746) for each of the evidential layers used.

3.2. Training and validation datasets

The use of bivariate statistical modelling in a data-driven based mineral potential mapping essentially thrives on the presence of known locations of the mineral, whose spatial distribution (in terms of their respective X and Y coordinates) is to be determined over a region of

interest. Hence, 181 locations of known gold occurrences, which have been derived from historically mapped locations of artisanal mining operations as well as locations of anomalously high Au geochemical assay values in parts per billion (obtained from Azumah Resources Limited), were analogously converted to obtain a total Au pixels of 723 counts. These Au occurrences were used to train and validate the mineral prospectivity models to be produced. A proportion of the known locations of gold occurrences (equal to seventy percent) were employed in the training of the predictive models generated and are thus referred to as training data. The remaining thirty percent of the known gold locations were used to validate the predictive models produced based on the use of the data-driven bivariate methods discussed under Section 3.3.

3.3. Data-driven geospatial models

In this study, predictive models generated for the favourable zones of mineral occurrence over the Collette PL Area were carried out using two bivariate statistical models comprising the statistical index and the weighting factor.

3.3.1. Statistical index (SI) model

In terms of geospatial modelling, the introduction of the statistical index as a bivariate statistical modelling technique was first employed in the delineation of susceptible zones of landslide occurrences by Van Westen (1997). For its employability in geospatial modelling, this method essentially requires that a geospatial modeller selects and maps the relevant locations of a known natural resource or hazard (in this study, gold occurrence) with respect to various classes within a chosen evidential layer (Khosravi et al., 2016). In this study, this was carried out by overlaying the training data on each of the eight evidential layers, which have been discretised into their respective classes. Thus, for each class of an evidential layer, SI-based weight values obtained are the natural logarithm of the intensity of occurrence of gold mineral within that class divided by the total mineral intensity of the study area. The SI method and its implementation are summarised in the expression shown in equation (1), as introduced by Van Westen (1997).

$$W_{SI} = \ln\left[\frac{M_{ij}}{M}\right] = \ln\left[\frac{Au_{ij}/Au_T}{A_{ij}/A_T}\right] \tag{1}$$

From equation (1), W_{SI} denotes the SI-based weight that is computed for each class i of and evidential layer j; M_{ij} depicts the intensity of mineral occurrence within a chosen class i of an evidential layer j; M represents the total intensity of mineral occurrence within the evidential layer. Au_{ij} captures the number of known gold (Au) occurrences (training data) within class i of a given evidential layer j; Au_T comprises the total number of known Au occurrences within the training data; A_{ij} is the areal size of class i of a chosen evidential layer j and A_T represents the total areal size of the evidential layer j.

For each class i of an evidential layer j, a positive W_{SI} value attained is an indication that the known locations of Au mineral and the aforementioned class i are properly and robustly associated. Negative values of a computed W_{SI} means there is a poor or weak relationship between locations of known Au occurrences and class i of a given evidential layer j. No relationship or correlation is established between class i of a given evidential layer and the known location of Au occurrence if no training data is found in the said class i. When generating a mineral prospectivity model based on the statistical index method, each class within a given evidential layer is assigned their respective W_{SI} value. Afterwards, all the evidential layers are synthesised to generate the SI-based MPM as shown in equation (2).

$$MPM_{SI} = \sum_{j=1}^{n} W_{SI,ij} \tag{2}$$

Where MPM_{SI} denote the mineral prospectivity map generated based on the statistical information technique, n is the total number of evidential layers, and i represents the classes in each evidential layer j.

3.3.2. Weighting factor (WF) model

The weighting factor modelling method, which was first introduced by Cevik and Topal (2003), is a modified edition of the statistical index method, which has been employed successfully in geospatial modelling (Meinhardt et al., 2015; Khosravi et al., 2016). This is because, in carrying out the weighting factor method, weights determined are based on the utilisation of the W_{SI} values obtained. In carrying out the weighting factor technique for an i-th class of a given evidential layer, the total weighting index value for that class (TS_i is determined as a product of the class W_{SI} value and the number of pixels associated with the known Au occurrences within the said class i (as shown in equation (3)). Thus, for a class i in a given evidential layer j, the TS_i represents the rank of the class i among all the other classes within the evidential layer.

$$TSI_i = \sum_{i=1}^{n} \left\{ N_{pix}\left(Au_{ij} \times W_{SI}\right) \right\} \tag{3}$$

Where $Npix$ (Au_{ij}) is the number of pixels of known Au occurrences within class i and n represents the number of classes within the chosen evidential layer. Afterwards, the weight factor of each of the evidential layers j to be synthesised is generated based on the min-max approach as shown in equation (4).

$$WF_i = \frac{TS_i - \min TS_i}{\max TSI_i - min\ TS_i} \times 9 + 1 \tag{4}$$

The expression in equation (4) stretches the values of each evidential layer to a range of 1–10. min TS_i and max TS_i represent respectively the minimum and maximum values of the total weighting index. Thus, in the generation of the mineral prospectivity model based on the weighting factor method, each of the evidential layers used was multiplied by its corresponding weighting factor value; after which all the weighted evidential layers were integrated in a GIS environment as expressed in equations (5) and (6).

$$MPM_{WF} = \sum_{j=1}^{n} EV_{norm,j} \times WF_i \tag{5}$$

$$EV_{norm,j} = \frac{EV_i - EV_{\min}}{EV_{\max} - EV_{\min}} \tag{6}$$

where MPM_{WF} is the mineral prospectivity model generated based on the weighting factor model. $EV_{norm,j}$ denotes a normalised evidential layer, EV_{min} and EV_{max} represent the minimum and maximum values within a particular evidential layer, EV_i.

3.4. Validation of the mineral prospectivity models

An important task in carrying out mineral prospectivity modelling over this study area was to validate the predicted model outputs. In the geoscientific sense, the geospatial models produced are not of much essence and are without any meaningful relevance unless they are validated (Bourenane et al., 2016). In this study, the validation process was carried out based on the application of the receiver operating characteristics (ROC) curve. During the use of the ROC technique, the known location of Au occurrence (validation data) was matched with the mineral prospectivity models produced. This results in the determination of the distribution of Au validation data in comparison with the value classes of the generated mineral prospectivity models to ascertain the percentage of gold occurrences that align with the highly prospective zones. Values obtained from the employability of the ROC curve technique range from 0.5 to 1. For a particular model, a computed ROC value that is closer to 1 is an indication that the model produced has good and higher accuracy.

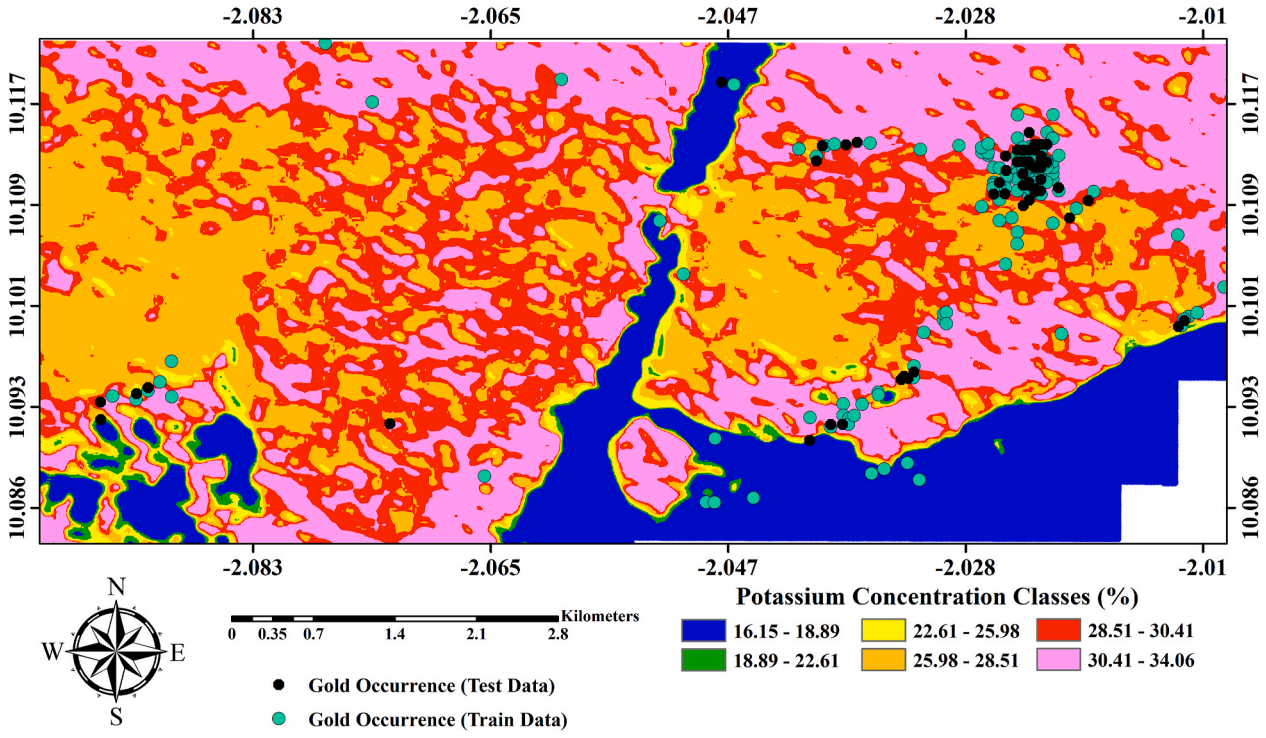

Fig. 4. Discretised map of the potassium concentration layer showing the spatial distribution of potassium within the Collette PL Area.

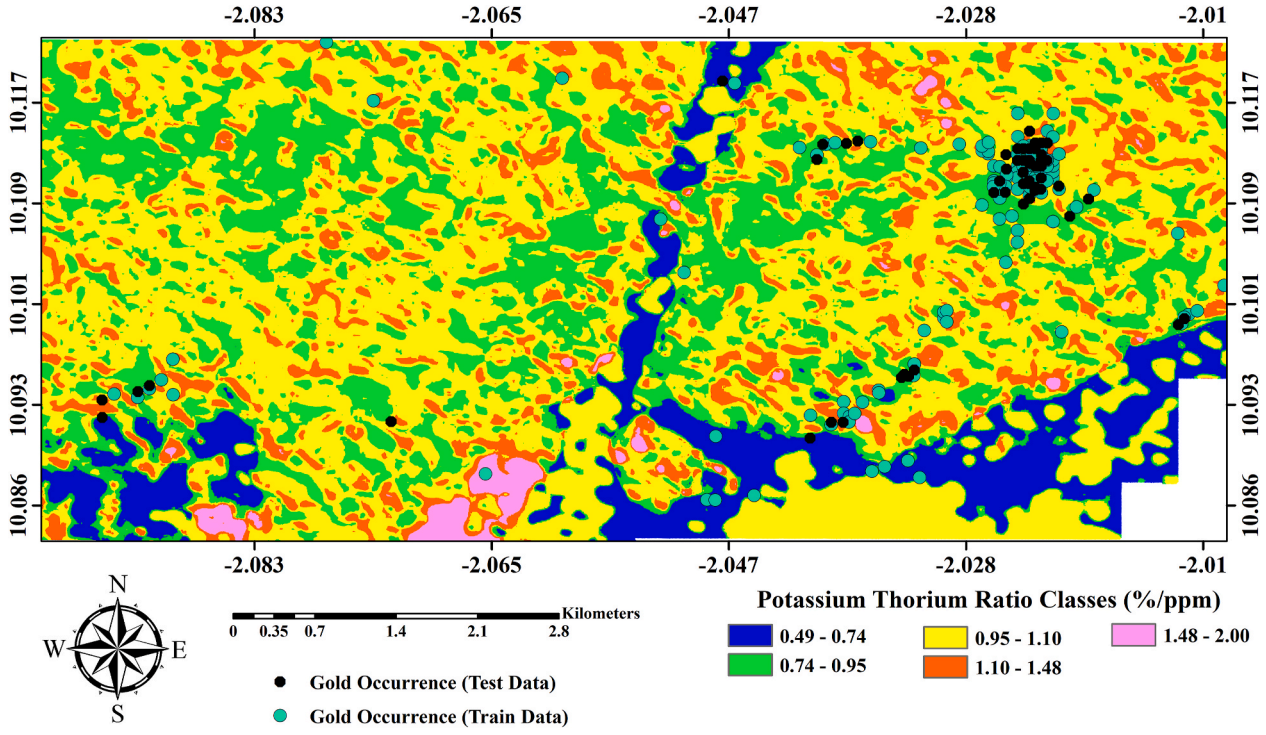

Fig. 5. Discretised map of the potassium-thorium ratio layer over the Collette PL Area.

4. Results and discussion

4.1. Characteristics of geoscientific evidential layers generated

The creation of predictive models over the study area using the weighting factor (WF) and the statistical index (SI) techniques to delineate prospective zones viable for the mineral occurrence was carried out by employing eight geospatial evidential layers sourced from radiometric (layers derived comprised potassium concentration, uranium concentration, potassium-thorium ratio, and uranium-thorium ratio layers), magnetic (layers extracted consist of the analytic signal, lineament density, and reduction-to-equator evidential layers), and geological (from which the geology layer was derived) datasets. In mineral prospecting, the use of evidential layers sourced from

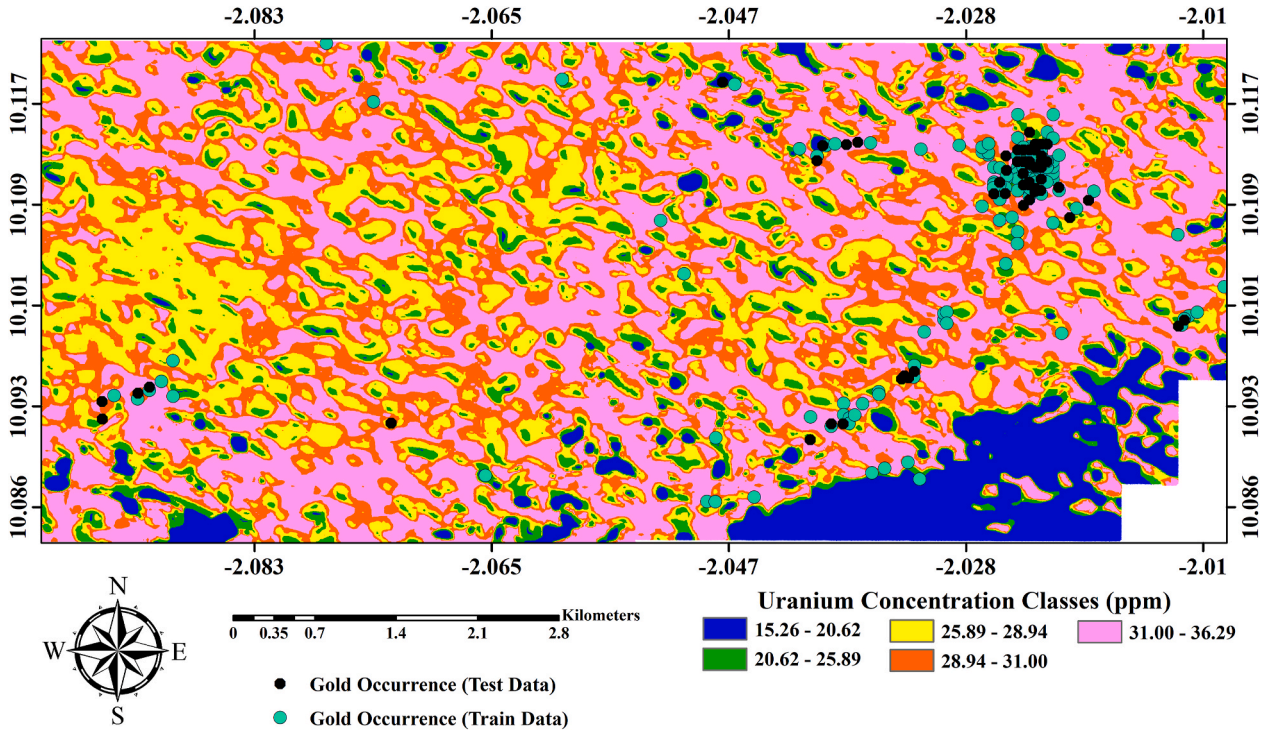

Fig. 6. Discretised map of the uranium concentration layer showing the spatial distribution of uranium over the Collette PL Area.

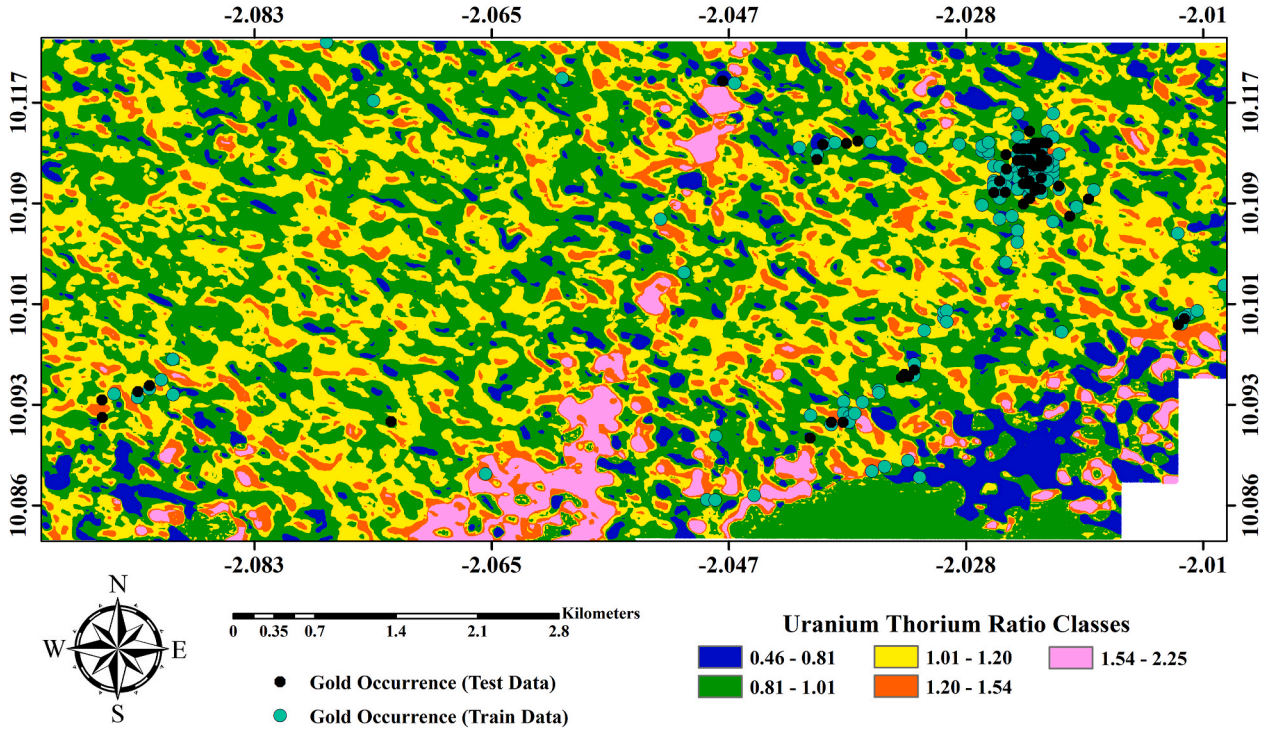

Fig. 7. Discretised map of the uranium-thorium ratio layer over the Collette PL Area.

radiometric data is very useful because of their ability to delineate alteration zones with enormous relevance to mineralisation over a designated area. Furthermore, in hydrothermal alteration zones, an enhancement or depletion is observed in practically every integration of potassium, thorium, and uranium (the three main radiometric elements). It is noteworthy that potassium enrichment is observed in situations of intense hydrothermally altered zones, and thus it reduces with respect to distance from a mineralisation region (Dentith and Mudge, 2014; Forson et al., 2021). Also, potassium-thorium antagonism, which arises due to the enhancement of potassium and depletion of thorium over a specified area, is an indication of a possible occurrence of mineralisation. Regions with increased uranium concentrations point to the possible occurrence of mineralisation. In terms of the uranium-thorium ratio, areas observed to be highly anomalous suggest the possible

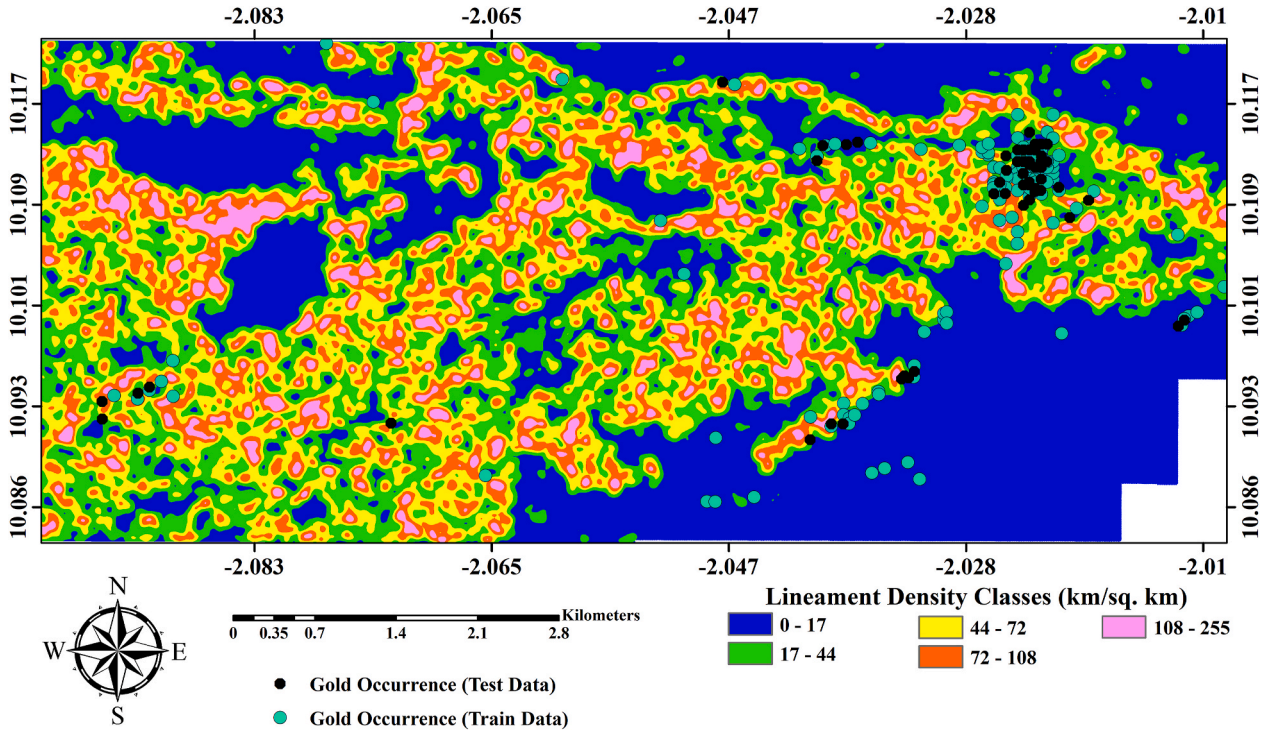

Fig. 8. Discretised map of the lineament density layer showing the intensity of occurrence of lineaments over the Collette PL Area.

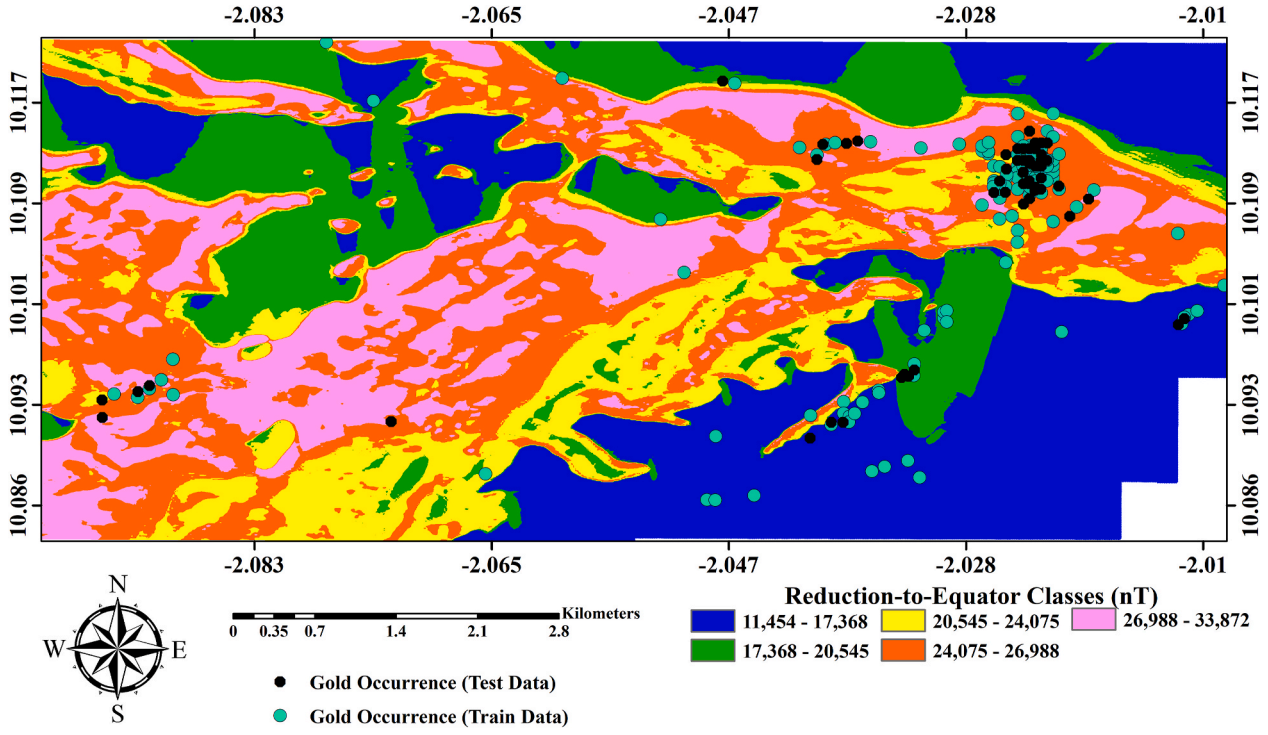

Fig. 9. Discretised map of the RTE-based magnetic intensity layer which depicts the distribution of magnetic intensity responses over the Collette PL Area.

occurrence of mineralisation and are deemed worthy target zones (Dentith and Mudge, 2014). Thus, for the four radiometrically-sourced layers, only the potassium concentration layer (shown in Fig. 4) was discretised into six classes, with the rest (potassium-thorium ratio, uranium, and uranium-thorium ratio) discretised into classes of five as shown in Figs. 5–7, respectively, using the Jenks natural breaking classification technique (Jenks, 1963; Chen et al., 2013). The lineament density layer (shown in Fig. 8) was sourced from the use of the CET (Centre for Exploration Targeting) grid analysis technique on the magnetic data over the study area. This layer outlines the intensity of geological structure occurrences within various regions over a specified area and thus depicts the extent of the endowment of various fracture zones within a geologic environment. Lineament density is essential in mineral prospecting because it characterises low-pressure zones, which

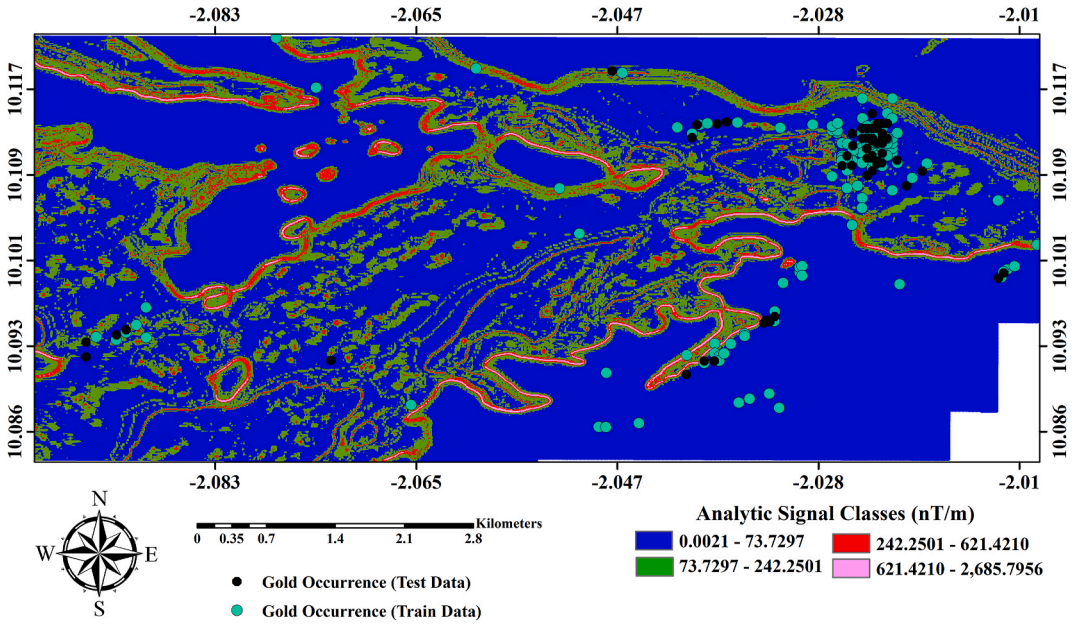

Fig. 10. Discretised map of the analytic signal layer depict the spatial distribution of magnetic intensity gradient over the Collette Area.

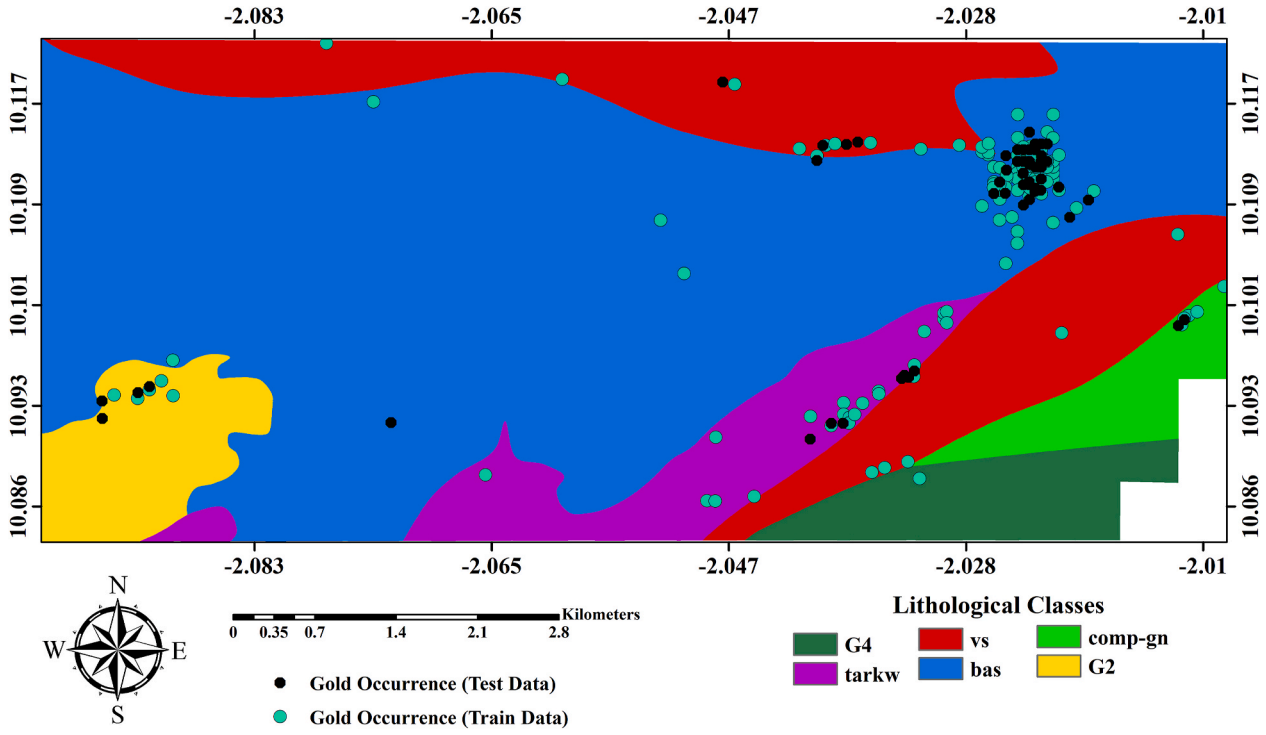

Fig. 11. Map of showing geology layer showing various lithological classes characterising the Collette PL Area.

act as conduits or points of convergence for hydrothermal fluids (Forson et al., 2020, 2021). Gold mineralisation occurrences within the Collette PL Area and north-western Ghana are generally related to quartz veins (made up of various structural features such as faults, dykes, etc.) (Amponsah et al., 2016). Thus, the lineament density layer (shown in Fig. 8) was classified into five classes. The spatial distribution of magnetic responses is very essential towards delineating prospective zones of mineral occurrence because mineral occurrence within the study area is strongly related to indicator minerals with a magnetic character such as arsenopyrite, pyrite, and magnetite. Hence, the inclusion of evidential layers that outline the distribution of magnetic responses within the study area was vital. In low magnetic latitude regions such as the north-western part of Ghana, within which this study was undertaken, the magnetic intensity responses observed are generally not characteristic of subsurface geology due to asymmetric problems that are associated with magnetic data acquired over low magnetic latitudes (Forson et al., 2021). Hence, the magnetic intensity data was reduced-to-equator (RTE) to make the observed magnetic intensity responses characteristic of subsurface geology. This resulted in the generation of the reduction-to-equator evidential layer shown in Fig. 9. This task carried out by the RTE was analogously carried out by the analytic signal (AS) filtering technique to generate geologically-characteristic magnetic

Table 1
Statistical Index and Weighting Factor scores of the Geoscientific evidential layers used.

EVs	Class	Total Number of Pixels	Au occurrence pixels	SI	WF
Geological Layer	G4	490,039	4	−1.7593	1
	tarkw	771,629	84	0.8312	
	vs	2,015,277	72	−0.2829	
	bas	6,447,210	304	−0.0055	
	comp-gn	356,547	20	0.1682	
	G2	549,870	20	−0.265	
Analytic Signal Layer (nT m^{-1})	0.0021–73.7297	7,927,794	428	1.1387	8.66
	73.7297–242.2501	2,199,613	68	0.6521	
	242.2501–621.4210	421,134	4	0.2003	
	621.4210–2.685.7956	82,031	4	1.0285	
RTE Layer (nT)	11,454–17,368	3,084,187	88	−0.5078	2.47
	17.368–20.545	1,710,402	44	−0.6114	
	20.545–24.075	1,561,787	32	−0.8389	
	24.075–26.988	2,605,859	296	0.8738	
	26,988–33,872	1,668,337	44	−0.5865	
Lineament Density Layer (km^{-2})	0–17	4,109,889	192	0.9854	8.68
	17–44	2,500,998	152	1.2819	
	44–72	2,220,323	116	1.102	
	72–108	1,325,318	40	0.6366	
	108–255	474,044	4	1.178	
Potassium Concentration Layer (%)	16.15–18.89	1,730,023	40	0.4877	10
	18.89–22.61	144,889	0	0	
	22.61–25.98	299,118	0	0	
	25.98–28.51	2,802,809	88	0.6622	
	28.51–30.41	2,635,542	140	1.1204	
	30.41–34.06	3,018,191	236	1.6493	
Potasium-Thorium Ratio Layer (%/ppm)	0.49–0.74	1,033,728	36	0.7346	8.38
	0.74–0.95	2,687,025	156	1.2246	
	0.95–1.10	5,533,838	264	1.0062	
	1.10–1.48	1,234,104	44	0.752	
	1.48–2.00	141,877	4	0.5947	
Uranium Concentration Layer (ppm)	15.26–20.62	894,701	16	0.3772	8.82
	20.62–25.89	839,547	40	1.0049	
	25.89–28.94	2,355,978	76	0.6804	
	28.94–31.00	2,572,949	132	1.0821	
	31.00–36.29	3,967,397	240	1.2759	
Uranium–Thorium Ratio Layer	0.46–0.81	896,673	48	1.1291	8.76
	0.81–1.01	4,687,297	268	1.206	
	1.01–1.20	3,697,917	164	0.9354	
	1.20–1.54	964,729	24	0.5247	
	1.54–2.25	383,956	0	0	

intensity gradients over the study area (captured on the analytic signal layer in Fig. 10). Although the analytic signal and the reduction-to-equator correct and mitigate the asymmetric effects in low magnetic latitude regions, the former does not take into account the direction of magnetisation. The RTE and AS evidential layers were discretised respectively, into classes of four and five for the implementation of the bivariate data-driven methods. Geologically, the Collette PL Area is generally characterised by six lithological classes consisting of bas (basalts), comp-gn (composite gneisses), G2 (granodiorite with diorite), G4 (granite and granodiorite), tarkw (Tarkwaian sediments), and vs (volcanosedimentary rocks) as shown in Fig. 11.

4.2. Mineral prospectivity models

4.2.1. Statistical index-based mineral prospectivity model

By employing the statistical index model, the scores obtained for each class of various geoscientific layers are shown in Table 1. Based on the results in Table 1, four geological layer classes consisting of bas, G2, G4, and vs were observed to have their computed SI scores being, respectively, −0.0055, −0.2650, −1.7593, and −0.2829. The negative scores obtained for the aforementioned lithological classes indicate a weak correlation with respect to the known gold occurrences within the study area. The geology of the Collette PL Area is dominated by comp-gn (composite granite and gneissess; 2196 - 2193 Ma) with a klipper of volcaniclastic rocks (mainly composed of siltstone and shale facies; 2139 Ma), G2 (tonalite and granitoid), and G4 (granitoids; 2111 ± 7 Ma) rocks. The Comp-gn with klipper of volcanosedimentary rocks has experienced intense *E*-W shearing, mylonitization with steep dips, and isoclinal folds with their axial planes parallel to the shear foliation as a result of thrust-related deformation (Amponsah et al., 2015). These shear zones have permitted the plumbing of hydrothermal fluids, creating wall rock alteration haloes. The widespread alteration within volcanosedimentary rocks consists of graphitization, silicification (quartz veining), sulphidation (mainly arsenopyrites and pyrites), and that of the comp-gn is associated with potassic alteration that accompanied the gold mineralisation. The intense zone of shearing is approximately 150 m in width. Also, the Tarkwaian sediments (2120 Ma) of quartzites and matured diamictite conglomerates are molassic sediments of the Comp-gn (granite and gneisses) and the volcaniclastic rocks and therefore may carry free gold around the valves of the pebble clast in the conglomerates (Nunoo et al., 2022). For this reason, Tarkw and comp-gn have a correlation with gold and a positive statistical value. G2 and G4 are late intrusions which usually occur as rounded moulds and intrude the early comp-gn and tarkw sediments with no association with gold mineralisation or sulphidation. The relevance of the two lithological classes with class names tarkw and comp-gn were deemed to be strong towards gold mineralisation occurrence within the study area due to the positive SI score obtained (which are respectively 0.8312 and 0.1682). In the case of the four-classified analytic signal layer, statistical index scores obtained for all the classes with range of values 0.0021 nT m^{-1} - 73.7297 nT m^{-1}, 242.2501 nT m^{-1} - 621.4210 nT m^{-1}, 73.7297 nT m^{-1} - 242.2501 nT m^{-1} and 621.4210 nT m^{-1} - 2.685.7956 nT m^{-1} were respectively 1.1387, 0.6521, 0.2003 and 1.0285. The SI scores obtained for the classes within the analytic signal

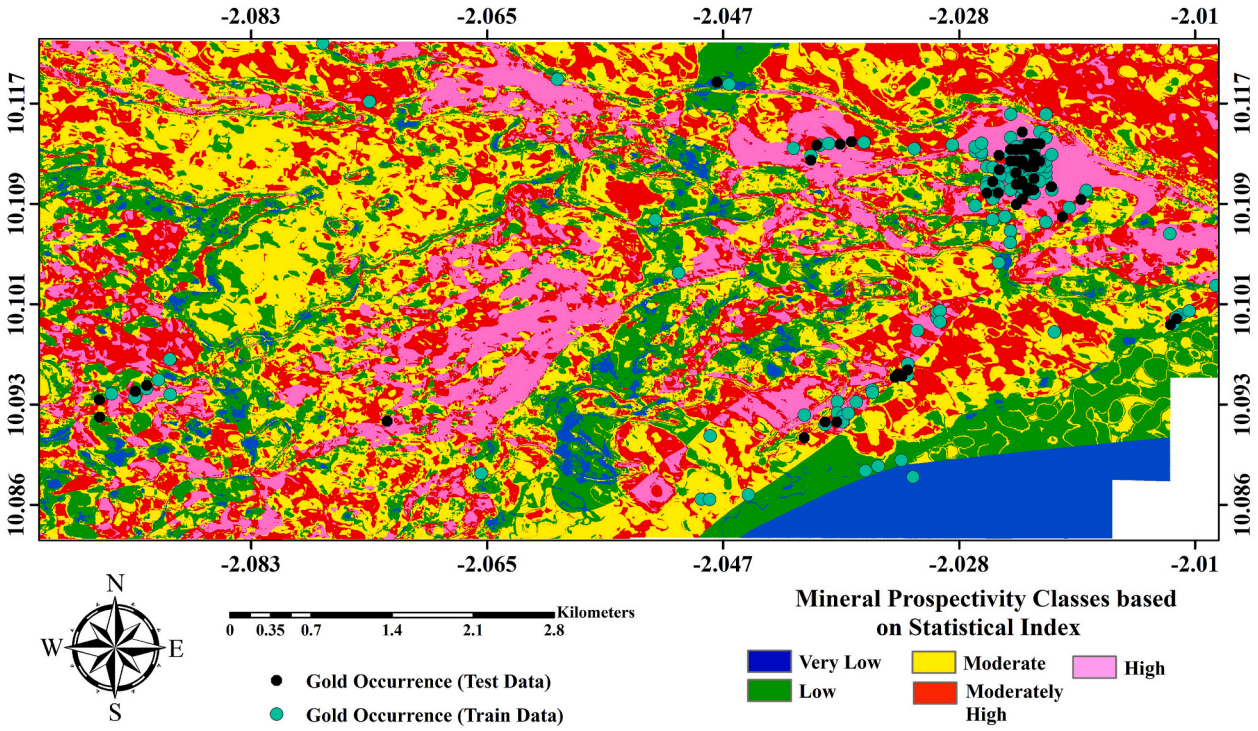

Fig. 12. Statistical index-based mineral prospectivity model.

layer mean that each of these classes has a strong correlation with respect to the known gold occurrences within the study area. In the case of the reduction-to-equator evidential layer, four out of the total five classes with a range of magnetic intensity values of 11,454 nT - 17,368 nT, 17.368 nT–20.545 nT, 20.545 nT–24.075 nT, and 26,988 nT - 33, 872 nT were observed to show very weakened relevance towards the known gold occurrences within the study area with statistical index scores of −0.5078, −0.6114, −0.8389, and −0.5865 respectively. The RTE layer class with a magnetic intensity value of 24.075–26.988 nT showed a strong correlation with respect to the gold occurrences within the study area with a positive statistical index score of 0.8738. In the case of the lineament density layer, all five classes show a positive correlation to gold mineralisation occurrences within the study area because the statistical index values computed were all positive. It is, however, worth noting that the class with a lineament density range of 17–44 km km^{-2} was adjudged to be the class with the highest correlation to mineral occurrence within the study area with an SI score of 1.2819. In the case of the potassium concentration layer, two classes with concentrations of 18.89–22.61% and 22.61–25.98% were statistically analysed to show no correlation with the known gold occurrences within the study area, owing to the zero SI scores obtained. The other potassium concentration classes were found to exhibit a positive correlation with respect to gold occurrences. It can further be observed that potassium classes with high potassium concentration values showed a higher correlation to gold mineralisation within the study area and vice versa. This observation corroborates the literature assertion that potassium enrichment is evidence of intense hydrothermal alteration occurrence and an indication of a highly probable occurrence of mineralisation (Dentith and Mudge, 2014; Forson et al., 2021). For the potassium-thorium ratio layer, all five classes show a positive correlation to gold occurrence due to the positive SI values attained. For the uranium concentration layer, though all the five classes were observed to show a positive correlation to gold mineralisation occurrences within the study owing to the positive SI value computed, the classes with higher uranium concentration values (28.94–31.00 ppm and 31.00–36.29 ppm) were observed to have higher SI scores (1.0821 and 1.2759 respectively); an indication of a very strong correlation with respect to the known gold occurrences. This trend of uranium concentration values also corroborates the assertion that regions with high uranium concentrations suggest a highly possible occurrence of mineralisation (Dentith and Mudge, 2014). With the exception of the uranium-thorium class with a range of values of 1.54–2.25 which showed no correlation with respect to gold occurrences within the study area, the other four classes were observed to exhibit a positive correlation to gold mineralisation occurrences within the study area with positive SI values. The SI scores obtained were assigned to their respective classes and synthesised to generate the statistical index-based mineral prospectivity model (SI-based MPM). The aforementioned model (shown in Fig. 12) characterises five classes of mineral prospectivity zones within the study area. It can be observed that the very low, low, moderate, moderately high, and high prospective zones covered an area of 2.91 km^2, 8.72 km^2, 13.72 km^2, 11.30 km^2, and 5.83 km^2 respectively, as shown in Table 2.

Table 2
Area extent and percentage of mineral prospectivity classes.

MPM	Statistical Index		Weighting Factor	
Class	Area of class (km2)	Percentage (%)	Area of class (km2)	Percentage (%)
Very Low	2.91	6.85	2.61	6.14
Low	8.72	20.53	10.23	24.08
Moderate	13.72	32.3	11.2	26.37
Moderately High	13.3	26.6	14.9	35.08
High	5.83	13.72	3.54	8.33

4.2.2. Weighting factor-based mineral prospectivity model

Whereas the statistical index technique analysed and determined the spatial correlation of each class within a given evidential layer towards the gold occurrences in the generation of a mineral prospectivity model, the weighting factor technique was implemented to determine the influence of each of the evidential layers employed towards the generation of mineral prospectivity models over the study area based on the known

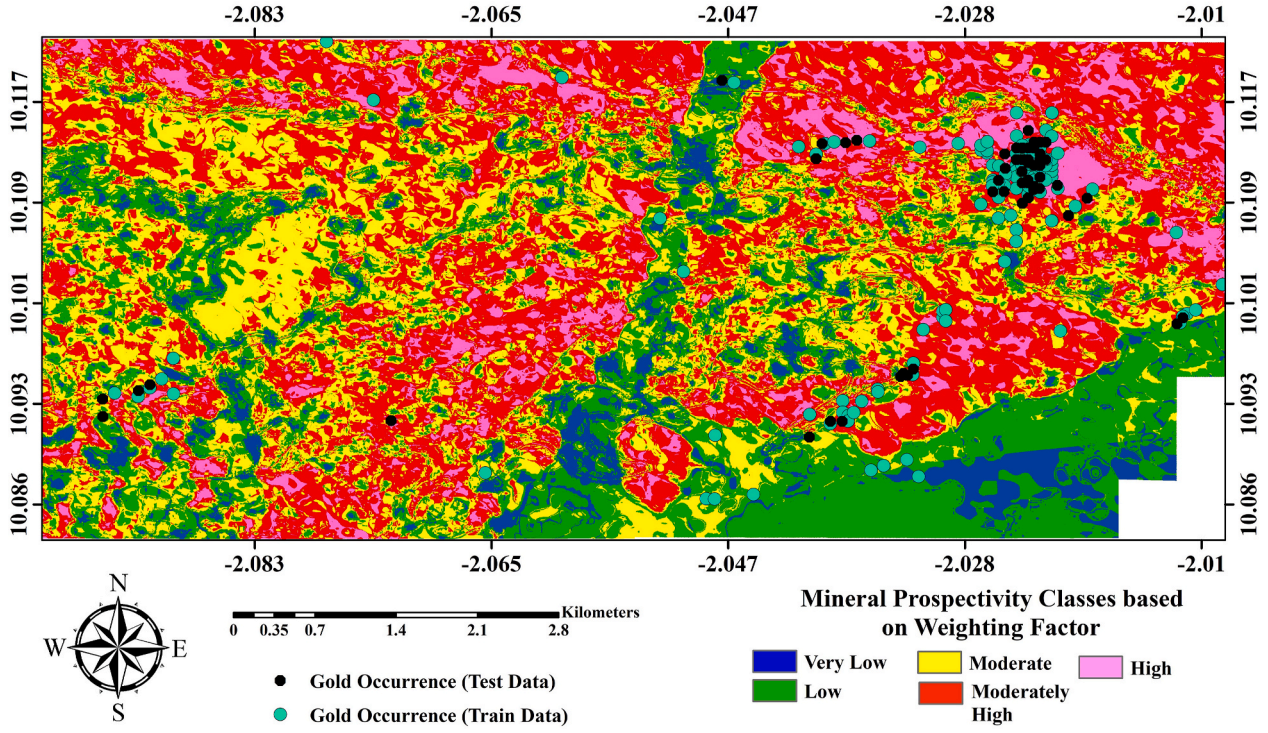

Fig. 13. Weighting factor-based mineral prospectivity model.

mineral occurrences used. The generation of weight factor scores for each of the eight geoscientific evidential layers was carried out based on the expression in equation (4). The weighting factor results obtained for the evidential layers ranged from 1 to 10; an evidential layer with a WF score of 1 is the layer with the least contribution towards the predictive model to be generated, whereas an evidential layer with a WF score of 10 has the highest influence on the mineral prospectivity model produced. Weighting factor scores obtained for the evidential layers in this study indicate that the potassium concentration layer and the lithological layer, respectively, have the highest and the least influence on the mineral prospectivity model produced based on the weighting factor technique (WF-based MPM). The WF scores obtained for the other six layers comprising reduction-to-equator, potassium-thorium ratio, analytic signal, lineament density, uranium-thorium ratio, and uranium were respectively 2.47, 8.38, 8.66, 8.68, 8.76, and 8.82. The WF-based MPM (shown in Fig. 13) was produced by multiplying each evidential layer by their respective WF scores and synthesising them. The resulting mineral prospectivity model in Fig. 13 has been discretised into five distinct classes of prospectivity using the Jenks natural breaking classification technique. From the output of the WF-based MPM, an area of 2.61 km^2, 10.23 km^2, 11.20 km^2, 14.90 km^2, and 3.54 km^2,respectively, was delineated to characterise the very low, low, moderate, moderately high, and high prospective zones of gold mineralisation within the study area (shown in Table 2).

4.3. Validation of the mineral prospectivity models produced

In mineral prospectivity modelling, an important task that ought not to be overlooked is the validation of predicted results. It is noteworthy that predictive models are less useful and lack any meaningful scientific relevance if they are not validated (Chung and Fabbri, 2003). In assessing the performance of a predictive model, the use of the receiver operating characteristics (ROC) curve has proven very useful and worthy of being applied. During the application of the ROC curve validation technique, known locations of gold occurrence data are compared with the MPM produced. Thus, the ROC curve quantitatively summarises the performance of a predictive model based on the area under the ROC curve (AUC), which indicates the efficacy of a constructed model for predicting a particular natural resource potential or geohazard susceptibility over an area of interest. AUC scores greater than 0.7 are considered efficient (Forson et al., 2022a). In this study, AUC based on ROC curves produced for the SI-based MPM (Fig. 14a) and WF-based MPM (Fig. 14b) using the training datasets of gold occurrence within the study area were found to be respectively 0.780 and 0.733. The AUC scores obtained indicate that the use of a statistical index for producing MPM provides a more accurate prediction in comparison with the weighting factor.

5. Conclusion

In the delineation of prospective zones of natural resource occurrence, various methods have been applied worldwide to synthesise various geospatial evidential layers in a data-driven manner. Popular among these data-driven methods are the statistical index and the weighting factor approaches. This study employed the statistical index and weighting factor approaches to prepare mineral prospectivity models over the Collette PL Area of the north-western part of Ghana using eight evidential layers sourced from magnetic, radiometric, and geological datasets. Furthermore, the predictive models produced based on these data-driven methods were compared to each other in this study. In the case of the statistical index technique, MPM was produced by assessing the coherence of each class within each of the eight evidential layers used with respect to the known location of gold mineralisation occurrences within the study area, based on the SI values obtained. For the weighting factor method, the MPM produced was preceded by the generation of individual weights for each of the eight evidential layers used by incorporating the known location of gold mineral occurrences within the study area. Results obtained for the SI-based MPM indicate that 6.85%, 20.53%, 32.30%, 26.60%, and 13.72% of the total area size of the study area were delineated as prospectively very low, low, moderate, moderately high, and high, respectively. For the weight factor-based MPM, the very low, low, moderate, moderately high, and high

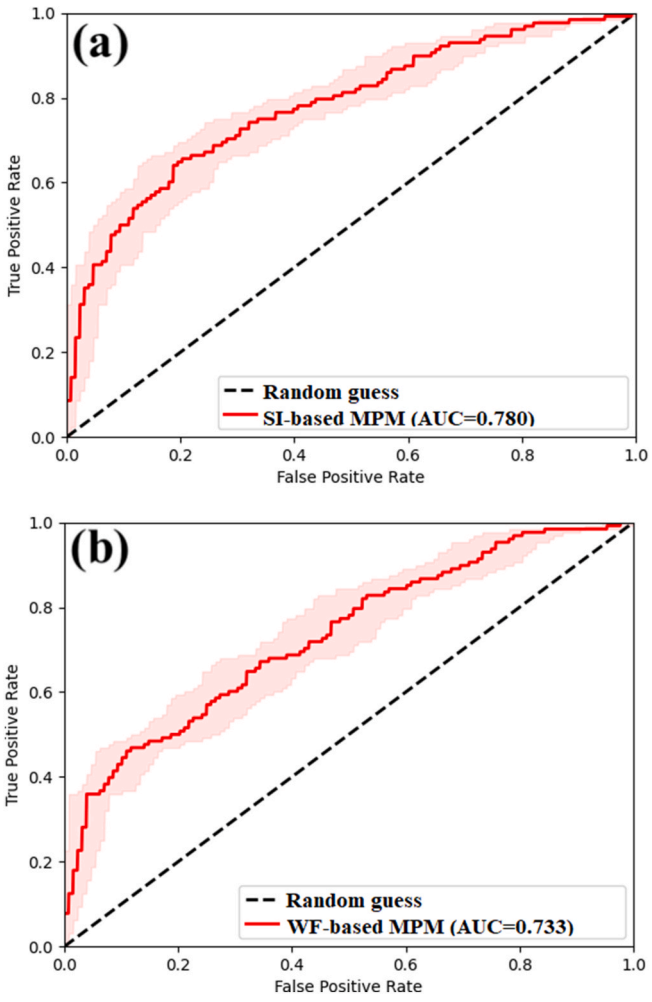

Fig. 14. Receiver operating characteristics (ROC) curve for **(a)** SI-based MPM **(b)** WF-based MPM.

prospective classes covered 2.61%, 24.08%, 11.20%, 14.90%, and 3.54% of the study area, respectively. By using the area under the receiver operating characteristics curve validation technique, the performance of the SI-based MPM and WF-based MPM produced were accordingly assessed to have AUC scores of, 0.780 and 0.733 respectively. The AUC scores obtained (greater than 0.7) indicate that the SI and WF models are good predictors of mineral occurrence potential over the study area. Based on the MPM outputs generated for the SI and WF, 19.13 km^2 and 18.44 km^2 were delineated as the highly probable zones (representing moderately high and high classes) of mineral occurrence over the Collette PL Area of north-western Ghana. It is also noteworthy to acknowledge that, these aforesaid data-driven spatial statistical techniques perform poorly or are non-functional in instances where known locations of mineral occurrences are rare or non-existent in the region to be studied.

Declaration of competing interest

The authors declare that they have no known competing financial interests or personal relationships that could have appeared to influence the work reported in this paper.

Data availability

Data will be made available on request.

Acknowledgements

The authors would like to thank Azumah Resources Limited for making the data available for this study. The authors are grateful to the University of Ghana-Carnegie Corporation and Building a New Generation Africa (BaNGA-Africa) for their immense support in making this study a success.

References

Abdelkareem, M., Al-Arifi, N., 2021. Synergy of remote sensing data for exploring hydrothermal mineral resources using GIS-based fuzzy logic approach. Rem. Sens. 13 (22), 4492.
Agra, N.A., Elburg, M.A., Vorster, C., 2023. Constraints on paleoproterozoic crustal growth from Birimian supergroup lavas of the bui belt (Ghana) in the west african craton. Precambrian Res. 384, 106926.
Agyei-Duodu, J., 2009. Geological Map of Ghana 1: 1 000 000. Geological Survey Department.
Akinlalu, A., Olayanju, G., Adiat, K., Omosuyi, G., 2021. Mineralisation potential assessment using analytical hierarchy process (AHP) modeling technique: a case study of ilesha schist belt, southwestern Nigeria. Results in Geophysical Sciences 7, 100026.
Al-Abadi, A.M., 2017. Modeling of groundwater productivity in northeastern Wasit governorate, Iraq using frequency ratio and shannon entropy models. Appl. Water Sci. 7 (2), 699–716.
Amponsah, P.O., Forson, E.D., Sungzie, P.S., Loh, Y.S.A., 2022a. Groundwater prospectivity modeling over the akatsi districts in the volta region of ghana using the frequency ratio technique. Modeling Earth Systems and Environment 1–19.
Amponsah, P.O., Salvi, S., Béziat, D., Siebenaller, L., Baratoux, L., Jessell, M.W., 2015. Geology and geochemistry of the shear-hosted julie gold deposit, nw Ghana. J. Afr. Earth Sci. 112, 505–523.
Amponsah, P.O., Salvi, S., Didier, B., Baratoux, L., Siebenaller, L., Jessell, M., Nude, P.M., Gyawu, E.A., 2016. Multistage gold mineralization in the wa-lawra greenstone belt, nw Ghana: the bepkong deposit. J. Afr. Earth Sci. 120, 220–237.
Amponsah, T.Y., Danuor, S.K., Wemegah, D.D., Forson, E.D., 2022b. Groundwater potential characterisation over the voltaian basin using geophysical, geological, hydrological and topographical datasets. J. Afr. Earth Sci. 192, 104558.
Amponsah, P.O., Kwayisi, D., Awunyo, E.K., Sapah, M.S., Sakyi, P.A., Su, B.X., Lu, Y., Nude, P.M., 2023. New evidence for crustal reworking and juvenile arc-magmatism during the Palaeoproterozoic Eburnean events in the Suhum Basin, South-east Ghana. Geol. J. In Press.
Azumah Resources Limited, 2018. The Julie Mineral Resource Estimate. Unpublished internal report.
Barati, M., Ostadhosseini, A., Rasa, I., Yazdi, M., 2018. Determination of cr geochemistry anomaly zones in the orzooiyeh area, hormozgan province using analytical hierarchy process (AHP). Journal of Economic Geology 10 (1), 47–59.
Baratoux, L., Metelka, V., Naba, S., Jessell, M.W., Grégoire, M., Ganne, J., 2011. Juvenile paleoproterozoic crust evolution during the eburnean orogeny (2.2–2.0 ga), western Burkina Faso. Precambrian Res. 191 (1–2), 18–45.
Block, S., Jessell, M., Aillères, L., Baratoux, L., Bruguier, O., Zeh, A., Bosch, D., Caby, R., Mensah, E., 2016. Lower crust exhumation during Paleoproterozoic (eburnean) orogeny, NW Ghana, West African craton: interplay of coeval contractional deformation and extensional gravitational collapse. Precambrian Res. 274, 82–109.
Bourenane, H., Guettouche, M.S., Bouhadad, Y., Braham, M., 2016. Landslide hazard mapping in the Constantine city, northeast Algeria using frequency ratio, weighting factor, logistic regression, weights of evidence, and analytical hierarchy process methods. Arabian J. Geosci. 9 (2), 1–24.
Carranza, E.J.M., 2008. Geochemical Anomaly and Mineral Prospectivity Mapping in GIS. Elsevier.
Carranza, E.J.M., 2015. Data-driven evidential belief modeling of mineral potential using few prospects and evidence with missing values. Nat. Resour. Res. 24 (3), 291–304.
Carranza, E.J.M., Laborte, A.G., 2015. Random forest predictive modeling of mineral prospectivity with small number of prospects and data with missing values in abra (Philippines). Comput. Geosci. 74, 60–70.
Cevik, E., Topal, T., 2003. Gis-based landslide susceptibility mapping for a problematic segment of the natural gas pipeline, Hendek (Turkey). Environ. Geol. 44 (8), 949–962.
Chen, J., Yang, S., Li, H., Zhang, B., Lv, J., 2013. Research on geographical environment unit division based on the method of natural breaks (jenks). Int. Arch. Photogram. Rem. Sens. Spatial Inf. Sci. 3, 47–50.
Chung, C.-J.F., Fabbri, A.G., 2003. Validation of spatial prediction models for landslide hazard mapping. Nat. Hazards 30 (3), 451–472.
Dentith, M., Mudge, S.T., 2014. Geophysics for the Mineral Exploration Geoscientist. Cambridge University Press.
Diatta, F., Ndiaye, P.M., Diène, M., Amponsah, P.O., Ganne, J., 2017. The structural evolution of the dialé-daléma basin, kédougou-kénièba inlier, Eastern Senegal. J. Afr. Earth Sci. 129, 923–933.
Dickson, K., Benneh, G., 1988. A New Geography of ghana. Longman group uk limited.
Eglinger, A., Thébaud, N., Zeh, A., Davis, J., Miller, J., Parra-Avila, L.A., Loucks, R., McCuaig, C., Belousova, E., 2017. New insights into the crustal growth of the paleoproterozoic margin of the Archean kéména-man domain, West African craton (Guinea): implications for gold mineral system. Precambrian Res. 292, 258–289.

Esmaeiloghli, S., Tabatabaei, S.H., Carranza, E.J.M., Hosseini, S., Deville, Y., 2021. Spatially-weighted factor analysis for extraction of source-oriented mineralization feature in 3d coordinates of surface geochemical signal. Nat. Resour. Res. 30 (6), 3925–3953.

Feng, X., Wang, E., Ganne, J., Amponsah, P., Martin, R., 2018. Role of volcano-sedimentary basins in the formation of greenstone-granitoid belts in the West African craton: a numerical model. Minerals 8 (2), 73.

Feng, X., Wang, E., Amponsah, P.O., Ganne, J., Martin, R., Jessell, M.W., 2019. Effect of pre-existing faults on the distribution of lower crust exhumation under extension: numerical modelling and implications for NW Ghana. Geosci. J. 23 (6), 961–975.

Ford, A., Miller, J.M., Mol, A.G., 2016. A comparative analysis of weights of evidence, evidential belief functions, and fuzzy logic for mineral potential mapping using incomplete data at the scale of investigation. Nat. Resour. Res. 25 (1), 19–33.

Forson, E.D., Amponsah, P.O., Hagan, G.B., Sapah, M.S., 2022a. Frequency ratio-based flood vulnerability modeling over the greater accra region of ghana. Modeling Earth Systems and Environment 1–20.

Forson, E.D., Menyeh, A., 2023. Best worst method-based mineral prospectivity modeling over the central part of the southern Kibi-Winneba belt of Ghana. Earth Science Informatics 1–20.

Forson, E.D., Menyeh, A., Wemegah, D.D., 2021. Mapping lithological units, structural lineaments and alteration zones in the southern Kibi-winneba belt of Ghana using integrated geophysical and remote sensing datasets. Ore Geol. Rev. 137, 104271.

Forson, E.D., Menyeh, A., Wemegah, D.D., Danuor, S.K., Adjovu, I., Appiah, I., 2020. Mesothermal gold prospectivity mapping of the southern kibi-winneba belt of Ghana based on fuzzy analytical hierarchy process, concentration-area (ca) fractal model and prediction-area (pa) plot. J. Appl. Geophys. 174, 103971.

Forson, E.D., Wemegah, D.D., Hagan, G.B., Appiah, D., Addo-Wuver, F., Adjovu, I., Otchere, F.O., Mateso, S., Menyeh, A., Amponsah, T., 2022b. Data-driven multi-index overlay gold prospectivity mapping using geophysical and remote sensing datasets. J. Afr. Earth Sci. 190, 104504.

Fu, C., Chen, K., Yang, Q., Chen, J., Wang, J., Liu, J., Xiang, Y., Li, Y., Rajesh, H., 2021. Mapping gold mineral prospectivity based on weights of evidence method in southeast asmara, Eritrea. J. Afr. Earth Sci. 176, 104143.

Ghasemzadeh, S., Maghsoudi, A., Yousefi, M., Mihalasky, M.J., 2022. Information value-based geochemical anomaly modeling: a statistical index to generate enhanced geochemical signatures for mineral exploration targeting. Appl. Geochem. 136, 105177.

Jenks, G.F., 1963. Generalization in statistical mapping. Ann. Assoc. Am. Geogr. 53 (1), 15–26.

Jessell, M.W., Amponsah, P.O., Baratoux, L., Asiedu, D.K., Loh, G.K., Ganne, J., 2012. Crustal-scale transcurrent shearing in the paleoproterozoic sefwi-sunyani-comoe region, west africa. Precambrian Res. 212, 155–168.

Kashani, S.B.M., Abedi, M., Norouzi, G.-H., 2016. Fuzzy logic mineral potential mapping for copper exploration using multi-disciplinary geo-datasets, a case study in seridune deposit, Iran. Earth Science Informatics 9 (2), 167–181.

Khosravi, K., Pourghasemi, H.R., Chapi, K., Bahri, M., 2016. Flash flood susceptibility analysis and its mapping using different bivariate models in Iran: a comparison between shannon's entropy, statistical index, and weighting factor models. Environ. Monit. Assess. 188 (12), 1–21.

Khosravi, V., Shirazi, A., Shirazy, A., Hezarkhani, A., Pour, A.B., 2021. Hybrid fuzzy-analytic hierarchy process (ahp) model for porphyry copper prospecting in simorgh area, eastern lut block of Iran. Mining 2 (1), 1–12.

Kusuma, K., Chaitanya, S., Guru, B., et al., 2019. Frequency ratio modelling using geospatial data to predict kimberlite clan of rock emplacement zones in dharwar craton, India. Int. J. Appl. Earth Obs. Geoinf. 74, 191–208.

Lin, N., Chen, Y., Liu, H., Liu, H., 2021. A comparative study of machine learning models with hyperparameter optimization algorithm for mapping mineral prospectivity. Minerals 11 (2), 159.

Mansouri, E., Feizi, F., Rad, A.J., Arian, M., 2017. A comparative analysis of index overlay and topsis (based on ahp weight) for iron skarn mineral prospectivity mapping, a case study in sarvian area, markazi province, Iran. Bulletin of Mineral Research and Exploration 155 (155), 147–160.

Masurel, Q., Eglinger, A., Thébaud, N., Allibone, A., André-Mayer, A.-S., McFarlane, H., Miller, J., Jessell, M., Aillères, L., Vanderhaeghe, O., et al., 2022. Paleoproterozoic gold events in the southern West African craton: review and synopsis. Miner. Deposita 57 (4), 513–537.

Mathew, T.G., Ariffin, K.S., 2018. Gold potential mapping in Kelantan (Malaysia) using ArcGIS and excel applying frequency ratio model. In: 2018 National Geoscience Conference.

McKay, G., Harris, J., 2016. Comparison of the data-driven random forests model and a knowledge-driven method for mineral prospectivity mapping: a case study for gold deposits around the huritz group and nueltin suite, nunavut, Canada. Nat. Resour. Res. 25 (2), 125–143.

Meinhardt, M., Fink, M., Tünschel, H., 2015. Landslide susceptibility analysis in central vietnam based on an incomplete landslide inventory: comparison of a new method to calculate weighting factors by means of bivariate statistics. Geomorphology 234, 80–97.

Nunoo, S., Hofmann, A., Kramers, J., 2022. Geology, zircon u–pb dating and εhf data for the julie greenstone belt and associated rocks in nw Ghana: implications for birimian-to-tarkwaian correlation and crustal evolution. J. Afr. Earth Sci. 186, 104444.

Parsa, M., Carranza, E.J.M., 2021. Modulating the impacts of stochastic uncertainties linked to deposit locations in data-driven predictive mapping of mineral prospectivity. Nat. Resour. Res. 30 (5), 3081–3097.

Rahimi, E., Shekarian, Y., Farahani, S., Asgari, G., Nakini, A., 2020. New approach in application of the ahp–fuzzy topsis method in mineral potential mapping of the natural bitumen (gilsonite): a case study from the gilan-e-gharb block, the kermanshah, west of Iran. Am. J. Eng. Appl. Sci. 13 (1), 96–110.

Rocci, G., 1965. Essai d'interpretation de mesures geochronologiques. la structure de l'ouest africain. Sci. Terre 10 (3–4), 461–478.

Sanusi, S.O., Amigun, J.O., 2020. Logistic-based translation of orogenic gold forming processes into mappable exploration criteria for fuzzy logic mineral exploration targeting in the kushaka schist belt, north-central Nigeria. Nat. Resour. Res. 29 (6), 3505–3526.

Salvi, S., Amponsah, P.O., Siebenaller, L., Béziat, D., Baratoux, L., Jessell, M., 2016. Shear-related gold mineralization in Northwest Ghana: the Julie deposit. Ore Geol. Rev. 78, 712–717.

Sapah, M.S., Agbetsoamedo, J.E., Amponsah, P.O., Dampare, S.B., Asiedu, D.K., 2021. Neodymium isotope composition of palaeoproterozoic birimian shales from the Wa-Lawra belt, north-west Ghana: constraints on provenance. Geol. J. 56 (4), 2072–2081.

Sun, T., Li, H., Wu, K., Chen, F., Zhu, Z., Hu, Z., 2020. Data-driven predictive modelling of mineral prospectivity using machine learning and deep learning methods: a case study from southern jiangxi province, China. Minerals 10 (2), 102.

Van Westen, C., 1997. Statistical landslide hazard analysis. Ilwis 2, 73–84.

Yousefi, M., Carranza, E.J.M., 2015. Prediction–area (p–a) plot and c–a fractal analysis to classify and evaluate evidential maps for mineral prospectivity modeling. Comput. Geosci. 79, 69–81.

Zhang, P., Zhang, Z., Yang, J., Cheng, Q., 2022. Machine learning prediction of ore deposit genetic type using magnetite geochemistry. Nat. Resour. Res. 1–18.

Zhang, S., Carranza, E.J.M., Wei, H., Xiao, K., Yang, F., Xiang, J., Zhang, S., Xu, Y., 2021. Data-driven mineral prospectivity mapping by joint application of unsupervised convolutional auto-encoder network and supervised convolutional neural network. Nat. Resour. Res. 30 (2), 1011–1031.

Zhang, Z., Zuo, R., Xiong, Y., 2016. A comparative study of fuzzy weights of evidence and random forests for mapping mineral prospectivity for skarn-type fe deposits in the southwestern fujian metallogenic belt, China. Sci. China Earth Sci. 59 (3), 556–572.

Zhenjie, Z., Qiuming, C., Jie, Y., Guopeng, W., Yunzhao, G., 2021. Machine learning for mineral prospectivity: a case study of iron-polymetallic mineral prospectivity in southwestern fujian. Earth Sci. Front. 28 (3), 221.